Thin Solid Films 520 (2011) 1063–1068

Contents lists available at SciVerse ScienceDirect

Thin Solid Films

journal homepage: www.elsevier.com/locate/tsf

Perhydropolysilazane derived silica coating protecting Kapton from atomic oxygen attack

Longfei Hu [b], Meishuan Li [a,*], Caihong Xu [c], Yongming Luo [c]

[a] Shenyang National Laboratory for Materials Science, Institute of Metal Research, Chinese Academy of Sciences, Shenyang 110016, China
[b] China Academy of Aerospace Aerodynamics, Beijing 100074, China
[c] Institute of Chemistry, Chinese Academy of Sciences, Beijing 100080, China

ARTICLE INFO

Article history:
Received 18 March 2011
Received in revised form 28 September 2011
Accepted 10 October 2011
Available online 15 October 2011

Keywords:
Perhydropolysilazane
Kapton
Atomic oxygen
Sol–gel
Erosion yield

ABSTRACT

By using surface sol–gel method with perhydropolysilazane (PHPS) as a precursor, a silica coating was prepared on a Kapton substrate as an atomic oxygen (AO) protective coating. The AO exposure tests were conducted in a ground-based simulator. It is found that the erosion yield of Kapton decreases by about three orders of magnitude after the superficial application of the coating. After AO exposure, the surface of the coating is smooth and uniform, no surface shrinkage induced cracks or undercutting erosion are observed. This is because that during AO exposure the PHPS is oxidized directly to form SiO_2 without through intermediate reaction processes, the surface shrinkage and cracking tendency are prohibited. Meanwhile, this PHPS derived silica coating also presents self-healing effect due to the oxidation of free Si. Compared with other kinds of silica or organic polymer coatings, this PHPS derived silica coating exhibits a superior AO erosion resistance.

1. Introduction

Atomic oxygen (AO) is the predominant environmental species in low earth orbit (LEO). In LEO space, AO can readily oxidize various space materials especially polymers, resulting in their performance degradation and even mission premature failure of the spacecrafts [1]. Therefore, many efforts have been made to develop protective coatings against AO erosion [2,3]. Thin oxide films such as SiO_2 and Al_2O_3 are typically applied as AO protective coatings due to their high stability under oxidative environment [4]. Generally, these coatings are prepared by physical vapor deposition method. However, most of these dryly-deposited coatings are brittle, and crack easily during storage, transportation and installation. These cracks will cause the undercutting erosion of the protected polymers during AO exposure [5,6]. Moreover, there are some difficulties to deposit this kind of dryly coatings on practical components with complex surface or big dimensions.

Wet process such as sol–gel method is also used to prepare thin oxide films of SiO_2 and Al_2O_3. This sol–gel method is simple and inexpensive, especially suitable for application on practical components with complex surface or big dimensions. Zhang and his coworkers [7,8] prepared SiO_2 and Al_2O_3 coatings on Kapton substrate using sol–gel method and investigated their AO resistance in a ground-based simulator. It has been found that these coatings could provide good AO resistance, the AO erosion yield of Kapton decreased by one or two orders of magnitude after the superficial application of SiO_2 or Al_2O_3. However, these coatings cracked in the process of AO exposure, undercutting erosion of the polymer substrate could be observed in high AO fluence exposure. In order to inhibit the undercutting erosion, the good flexibility and self-healing of protective coatings is also required apart from low AO erosion yield. Recently, a SiO_2 precursor, perhydropolysilazane (PHPS), has been synthesized [9–11]. The PHPS derived silica coatings are flexible and transparent, and their surfaces are free from deficiencies such as voids, pinholes and cracks [11]. It can be expected that during AO exposure, this kind of coatings may exhibit low AO erosion yield as well as good crack induced undercutting erosion resistance.

In this work, a PHPS derived silica coating was prepared through a surface sol–gel process on Kapton, a widely used space material [12]. The AO resistance of the coating was evaluated in a ground-based simulator, and the mechanism for the AO erosion resistance of the coating was discussed. This work is instructive for developing high performance AO erosion resistant coatings.

2. Experimental details

2.1. Coating preparation

PHPS ($H[SiH_2NH]_nSiH_3$, $M_n = 1500$), supplied by Institute of Chemistry, Chinese Academy of Sciences, was used as the SiO_2 precursor. Initially, the PHPS was diluted with xylene as a weight ratio of 5%, then this solution was mechanically stirred at room temperature for

* Corresponding author at: 72 Wenhua Road, Shenyang 110016, China. Tel.: +86 24 23971145; fax: +86 24 23891320.
E-mail address: mshli@imr.ac.cn (M. Li).

0040-6090/$ – see front matter © 2011 Elsevier B.V. All rights reserved.
doi:10.1016/j.tsf.2011.10.011

30 min to obtain a uniform and transparent solution. Kapton sheets with dimensions of 30 mm × 30 mm × 30 μm were selected as the polymer substrate in this experiment. The PHPS derived silica coating was prepared on Kapton substrate through a surface sol–gel process. Before applied coating, the substrate samples were degreased with acetone and ethanol initially, then activated in 1 M NaOH solution for 30 min and subsequently protonated in 0.1 M CH_3COOH solution for 30 min, finally rinsed with copious amount of distilled water and dried in clean air. The above treatment causes enrichment of –OH groups on the substrate surface, which benefits the superficial growth of the silica coating [13,14]. The PHPS derived silica coating was then deposited on these activated substrates through a surface sol–gel process, which involved four steps: (1) immersing the activated substrates in a PHPS solution (5 wt.%) for 1 min, (2) drying in clear air, (3) treating in vacuum furnace at 200 °C (Pressure <10 Pa), and (4) hydrolyzing with distilled water. The thickness of the as-prepared PHPS derived silica coating was about 0.5 μm.

2.2. Ground-based simulation facility and exposure test

The AO exposure experiments were performed in an electron cyclotron resonance type AO simulator. In this simulator, an AO beam with kinetic energy of about 5 eV was generated [15]. The effective fluence of the AO beam was calibrated using a standard method of ASTM E 2089–2000 [16,17]. Based on mass loss measurement of a standard Kapton H200 in the AO beam, AO fluence (F, atoms·cm^{-2}) can be calculated using the following formula:

$$F = \frac{\Delta M}{A \cdot \rho \cdot E_y} \quad (1)$$

Where, ΔM is the sample mass loss (g), A is the sample surface area (cm^2), ρ is the sample density (for standard Kapton H200, ρ = 1.42 g·cm^{-3}), and E_y is the sample erosion yield (for standard Kapton , $E_y = 3.0 \times 10^{-24}$ cm^3·atom^{-1}).

In order to know the mass change of a sample during the AO exposure, the sample was periodically removed from the vacuum chamber and weighed using the Sartorius BP211-D microbalance with an accuracy of 10^{-5} g. After weighing, the sample was rapidly returned to the vacuum chamber for continued AO exposure.

2.3. Characterization method

Infrared analysis of the coated samples was performed using a Fourier transform infrared spectrometer (FTIR, Spectrum one, Perkin-Elmer, U.S.A.). The FTIR spectra were obtained under a resolution of 4 cm^{-1} and average scans of 16 times. Optical properties of the coated samples were analyzed by a UV–vis spectrophotometer (Lambda 35, Perkin-Elmer, U.S.A.). The thermal stability was characterized by thermal gravimetric analysis (TGA) in a thermo-balance (Setsys 16/18, SETARAM, France). The sample mass change was recorded continuously during heating from room temperature to 800 °C at a rate of 10 °C/min in an argon or air atmosphere. The surface morphologies of the coatings were examined with a Supra 35 scanning electronic microscope (SEM, LEO, Oberkochen, Germany) at an accelerating voltage of 15 kV. A thin gold film was coated on the samples surface before SEM observation in order to prevent charge accumulation. The coating surface investigations were also performed with a CSPM-3100 atomic force microscope (AFM, benyuan, China) in contact mode. A gold coated ContGB-type tip was used, the resonance frequency of the AFM tip was 13 kHz, the elastic coefficient was 0.2 N/m, the tip radius was lower than 25 nm.

The surface compositions of the samples were investigated by an X-ray photoelectron spectrometer (XPS, ESCALAB 250, Thermo VG, U.S.A.) equipped with an Al K_α monochromatic source. The survey spot of 500 μm and the scanning step of 0.1 eV were selected. The acquired binding energy was calibrated by the value of C 1 s (284.6 eV). The data were recorded and deconvoluted by XPS-PEAK (version 4.1).

3. Results and discussion

3.1. Characterization of the PHPS derived silica coating

3.1.1. Surface morphologies

The as-prepared PHPS derived SiO_2 coating is carefully characterized before AO exposure. Fig. 1 presents the SEM images of the PHPS derived SiO_2 coating. In Fig. 1, the unhydrolyzed surface of the coating is rough and some defects can be found clearly, while the hydrolyzed surface is smooth and defects free. Similar phenomenon can also be found in the AFM images (Fig. 2). In Fig. 2, the average surface roughness of the coating decreases from 119 nm to 22 nm after hydrolysis in distilled water. In the coating preparation, the solvent could volatile from the uncured coating to form pores and contaminations on the coating surface. When the cured coating was subsequently treated in distilled water, the outmost layer of the coating was partially hydrolyzed to form colloid. Finally, the coating surface became smooth and uniform due to healing effect of colloid. Details about this hydrolysis process will be discussed below.

3.1.2. Surface compositions

Before and after hydrolysis, the surface compositions of the PHPS coating are investigated by an infrared spectrometer. As shown in Fig. 3, the unhydrolyzed PHPS film shows absorption bands at 3400 cm^{-1} (N–H), 2150 cm^{-1} (Si–H), 1180 cm^{-1} (N–H), and 840–1020 cm^{-1} (Si–O and Si–N), being in agreement with the bonding structure of the PHPS. And a small fraction of Si–OH is also found. After hydrolysis in distilled water, the relative intensity of the infrared absorbance bands of N–H, Si–H, and Si–N bonds decreases remarkably. And an absorption band appears at 1075 cm^{-1}, corresponds to Si–O vibration. Previous studies [9–11,18] indicated that the PHPS was sensitive to moisture. In atmosphere environment, the PHPS was partially hydrolyzed and transformed

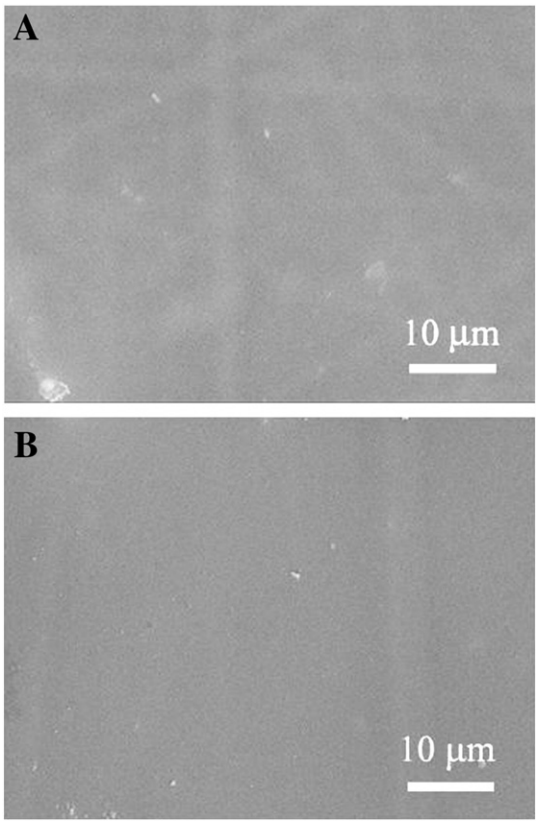

Fig. 1. SEM images of (a) original and (b) hydrolyzed PHPS coatings.

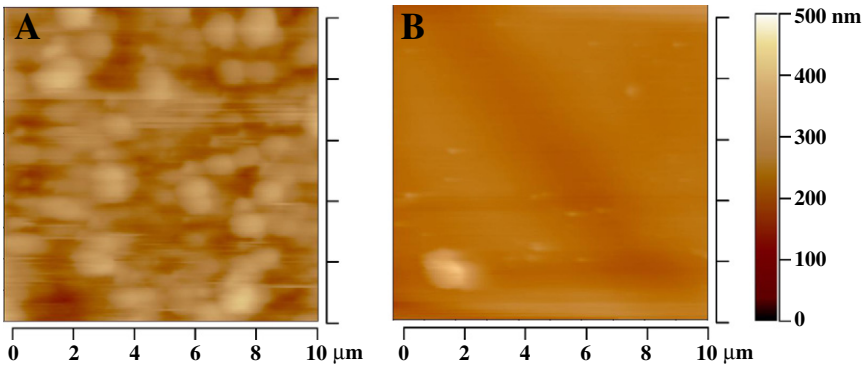

Fig. 2. AFM images of (A) original and (B) hydrolyzed PHPS coatings.

to $Si(OH)_4$ [18], which resulted in the breakage of Si – H,Si – N and N – H bonds. Furthermore, during hydrolysis in distilled water, $Si(OH)_4$ formed on the PHPS coating became unstable, easily decomposed to SiO_2 and H_2O. As a result, the main infrared absorbance band of the hydrolyzed coating corresponds to Si – O bond rather than Si – OH bond.

XPS analysis was performed to further identify the formation of SiO_2 on the prepared coating surface. As shown in Fig. 4, the survey spectra of the film display almost no variation after hydrolysis. High concentration N species can be found on the hydrolyzed surface, indicating that there is residual PHPS in the prepared coating. Prager et al. [19] found that the high conversion of PHPS to SiO_2 occurs only in the outer layer with a depth of 30 nm from the top surface. Beneath this outer layer, the conversion of PHPS to SiO_2 was negligible. When the outmost SiO_2 layer is thinner than 10 nm, the underlying PHPS can be detected in XPS analysis. This may be the main reason for detecting the high concentration of N species in the hydrolyzed coating. In high-resolution Si*2p* analysis, we can see that Si*2p* spectra are composed of three different peaks, which correspond to Si – N, Si – H, and Si – O bonds. For the unhydrolyzed coating, the main peak corresponds to Si – N bond, but for the hydrolyzed coating, Si – O bond became predominant. The binding energy of Si – O peak in the deconvoluted Si*2p* is 103.7 eV, quite close to the binding energy of Si – O bond in SiO_2 (103.6 eV) [20]. Therefore, it can be concluded that a thin SiO_2 layer has formed on the coating surface. Based on the related previous work [9,11], the possible reactions in the coating preparation can be described as following:

$$2Si{-}H + 8H_2O \rightarrow 2Si(OH)_4 + 5H_2 \quad (2)$$

$$Si(OH)_4 \rightarrow SiO_2 + 2H_2O \quad (3)$$

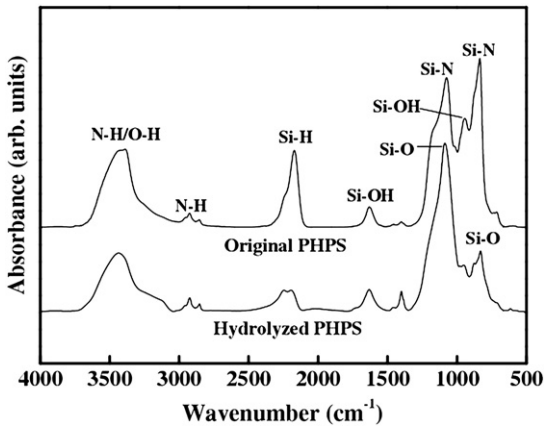

Fig. 3. FTIR spectra of original and hydrolyzed PHPS coatings.

3.1.3. Thermal stability

Thermal stability of the unhydrolyzed and hydrolyzed PHPS coatings has been evaluated through TG analysis, the results are shown in Fig. 5. It can be seen that the TG curves show different characters in Ar and air atmosphere. In Ar atmosphere, TG curves of the unhydrolyzed and hydrolyzed coatings coincide with each other, an apparent mass loss happened in the range from 200 °C to 400 °C. Their residual mass is about 93% at 800 °C. Iwamoto et al. [21,22] have pointed

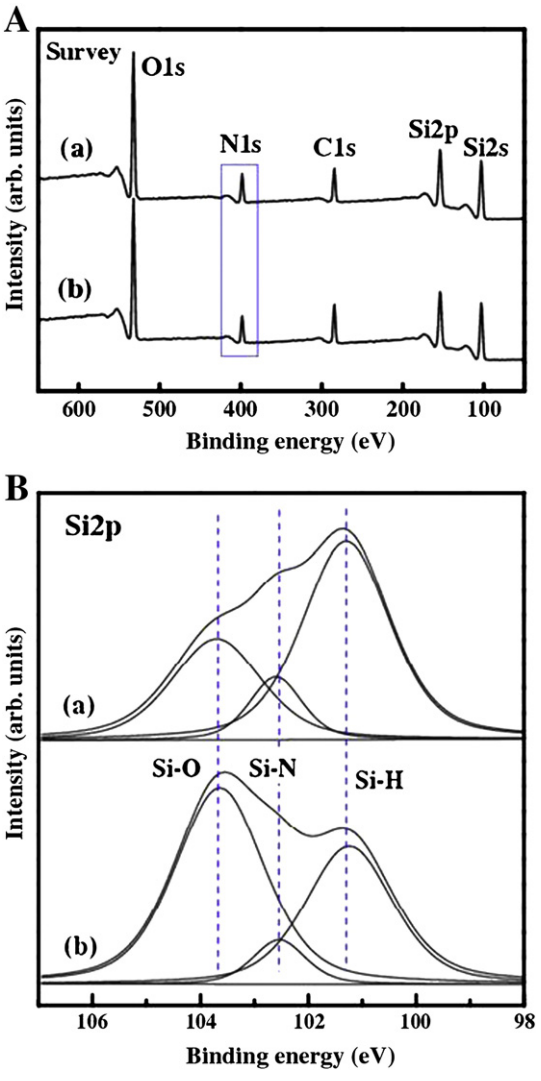

Fig. 4. XPS survey and high-resolution Si*2p* spectra of (A) original and (B) hydrolyzed PHPS coatings.

that the mass loss of the PHPS derived SiO_2 coating mainly resulted from the evaporation of residual solvent (xylene). As the unhydrolyzed and hydrolyzed coatings possess the same concentration of residual solvent, their total mass loss should be the same during thermal treatment in Ar at the same temperature. However, in air atmosphere, the mass loss evolution of the unhydrolyzed and hydrolyzed coatings is different, their residual mass is 88% and 95% at 800 °C, respectively. This is because that during thermal treatment in air, the residual xylene in the unhydrolyzed coating was oxidized to form a SiO_2 top layer, which could protect the hydrolyzed coating from further oxidation. As a result, the total mass loss of the hydrolyzed coating is much lower than that of the unhydrolyzed coating.

In a word, the surface sol–gel PHPS coating possesses very high inorganic remnant after thermal treatment in inert or oxidizing atmosphere. Hydrolysis in distilled water can promote the formation of a SiO_2-rich surface layer, which enhances the oxidation resistance of the PHPS coating. Therefore, the hydrolyzed coating, i.e. PHPS derived SiO_2 coating, is selected for further evaluation of its AO erosion resistance.

3.2. AO resistance of the PHPS derived SiO_2 coating in AO beam

3.2.1. Erosion kinetics

The AO exposure tests of pristine and coated Kapton were conducted for the total AO fluence of 9.3×10^{20} atoms·cm^{-2}. Their mass losses versus AO fluence are presented in Fig. 6. It can be seen that the mass loss of pristine Kapton increases linearly with AO fluence, indicating that it is not resistant to AO attacks. When Kapton is coated with the PHPS derived SiO_2 coating, the total mass loss decreases significantly from 3.8 mg·cm^{-2} to about 0.8×10^{-2} mg·cm^{-2} after AO exposure of 9.3×10^{20} atoms·cm^{-2}. In the whole AO exposure, the mass loss rate of the coated Kapton keeps at a negligible level. The calculated erosion yield of the coated Kapton is 6.0×10^{-27} cm^3·atom^{-1}, being three orders of magnitude lower than that of pristine Kapton (3.0×10^{-24} cm^3·atom^{-1}). Therefore, the PHPS derived SiO_2 coating can protect the Kapton substrate effectively from AO erosion.

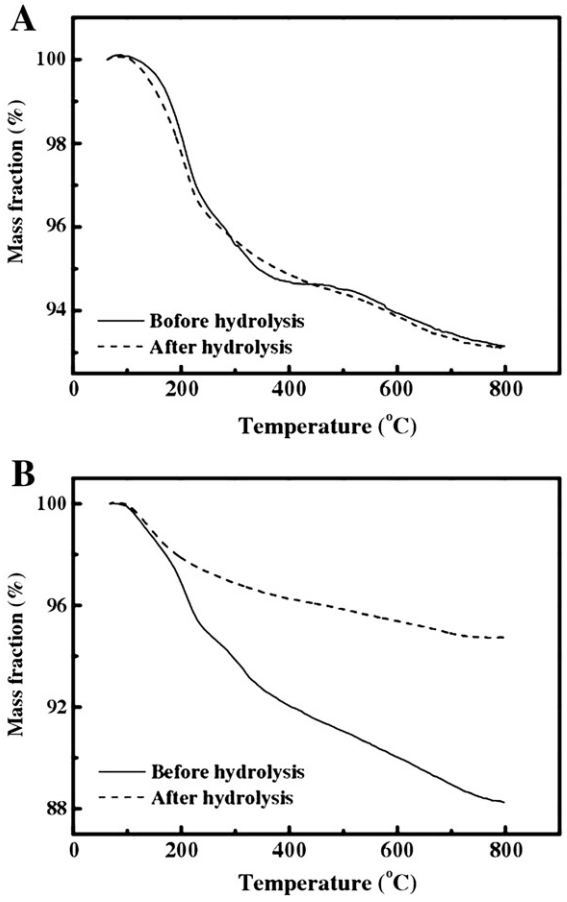

Fig. 5. TG curves of the as-prepared PHPS film before and after hydrolysis: (A) in Ar, (B) in air.

3.2.2. Surface morphology

Fig. 7 shows the SEM surface morphologies of the pristine and coated Kapton before and after AO exposure. Initially, the pristine Kapton has a smooth surface (Fig. 7A) and is transparent with a slight yellow color. After AO exposure, its surface exhibits a "carpet-like" structure (Fig. 7B), indicating the pristine Kapton has been severely eroded. This result is in agreement with that reported in the literature [23]. The original coated Kapton surface is uniform, no defects such as cracks and holes are visible. After AO exposure, some micro-pores appear on the coating surface (Fig. 7C), and their total number increased with exposure time. But these micro-pores do not further grow in their dimensions in the continued AO exposure, indicating no undercutting effect occurs. During AO exposure, the residual xylene in the PHPS derived coating is oxidized by incident oxygen atoms, and some micro-pores form. These micro-pores may become the path for AO to erode the underlying materials. On the other hand, the PHPS derived SiO_2 coating possesses self-healing property [9], which can inhibit the growth of micro-pores effectively. Thus, the PHPS derived SiO_2 coating still keeps its protectiveness even under the existence of surface defects. In order to identify the self-healing property of the coating, one coated sample is cracked through bending on a 2.0 mm diameter mandrel and then exposed in the same AO beam. The crack induced rapid erosion has not been found in the cracked region (Fig. 7D).

3.2.3. Surface compositions

The surface compositions of the pristine and coated Kapton were analyzed using XPS before and after AO exposure, the obtained data are list in Table 1. After AO exposure, the C content on the pristine Kapton decreases, conversely the O content increases, indicating that the Kapton has been eroded. The AO erosion of Kapton is mainly due to the oxidation of C species in the polymer structure, which has already been reported in some literatures [24,25]. The surface composition variations of the coated Kapton also show a similar trend. After AO exposure, the N content on the coated Kapton surface decreases from 9.1 at.% to 0.7 at.%, while the O content increases from 31.6 at.% to 48.8 at.%. The O-to-Si ratio on the exposed surface approaches to 2.0, equals the O-to-Si ratio of SiO_2. Therefore, the PHPS derived SiO_2 coating has been oxidized in the AO exposure and the dominated

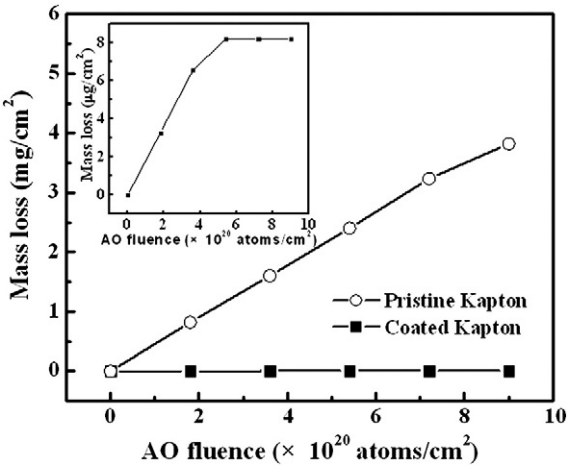

Fig. 6. AO erosion kinetics of pristine and coated Kapton, AO fluence = 9.3×10^{20} atoms·cm^{-2}.

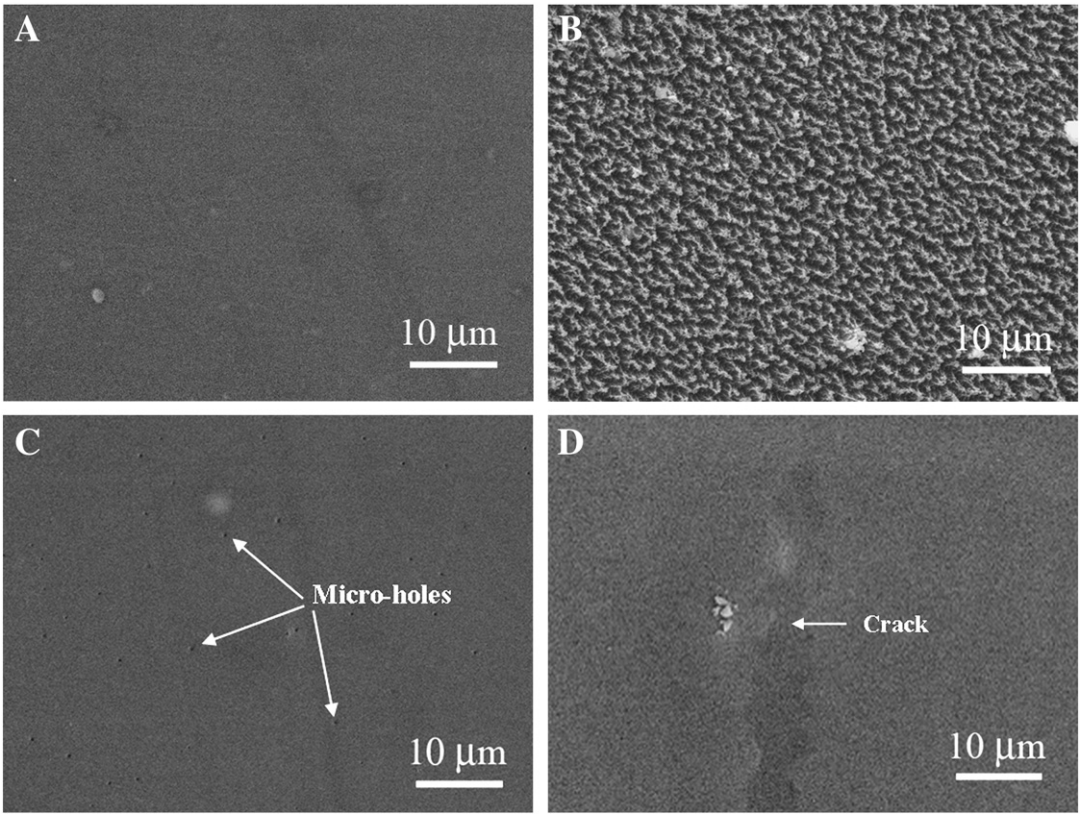

Fig. 7. SEM surface images of (A) original Kapton, (B) exposed Kapton, (C) exposed PHPS derived SiO_2 coating, showing the existence of surface holes, (D) exposed PHPS derived SiO_2 coating with pre-cracking treatment, showing no evidence of undercutting erosion under pre-existent cracks, AO fluence = 9.3×10^{20} atoms·cm^{-2}.

oxide formed on the coating surface is properly SiO_2. The formation of this SiO_2-rich surface layer can be further identified by the Si*2p* high-resolution analysis (Fig. 8). From Fig. 8, we can see that the Si*2p* spectrum is composed of a unique peak corresponding to Si – O bond. The binding energy of this peak is 103.6 eV, equal to the binding energy of Si – O bond in SiO_2 (103.6 eV). Obviously, SiO_2 forms on the coating surface during AO exposure [26].

3.2.4. Optical property

The UV–vis analysis was also performed to evaluate the AO effect on the optical property of the PHPS derived SiO_2 coating. Fig. 9 displays the transmittance curves of the pristine and coated Kapton before and after AO exposure of 9.3×10^{20} atoms·cm^{-2}. In Fig. 9, the pristine Kapton is infrared transparent in the wavelength of 0.5–1.1 μm. After AO exposure, the transitivity of Kapton decreases dramatically and its optical band gap shows an obvious red-shift, indicating that Kapton has been eroded in the AO beam. On the contrary, the coated Kapton still keeps high transparency after AO exposure. The transitivity decrement is only about 2%. As the Kapton is not resistant to AO attack, the surface became rough due to AO erosion. Therefore, the optical transitivity of the exposed Kapton decreases because the roughed surface enhances light scattering. However, the coated Kapton is resistant to AO erosion and the formed SiO_2-rich surface layer is smooth and transparent. Consequently, its transitivity exhibits a relatively lower decrement after AO exposure. It should be noted that initially the coated Kapton presents higher transitivity than the pristine Kapton. Similar phenomenon also has been reported in the literatures [27,28]. This phenomenon results from the anti-reflective effect of the surface coating.

Table 1
Surface compositions of the blank and coated Kapton before and after AO exposure, AO fluence = 9.3×10^{20} atoms·cm^{-2}.

Sample		Composition (at.%)				O/Si ratio
		C	N	O	Si	
Kapton	Before exposure	75.9	6.9	17.2	—	—
	After exposure	40.8	4.4	54.8	—	—
Coated Kapton	Before exposure	18.7	9.1	31.6	40.6	0.8
	After exposure	26.6	0.7	48.8	23.9	2.0

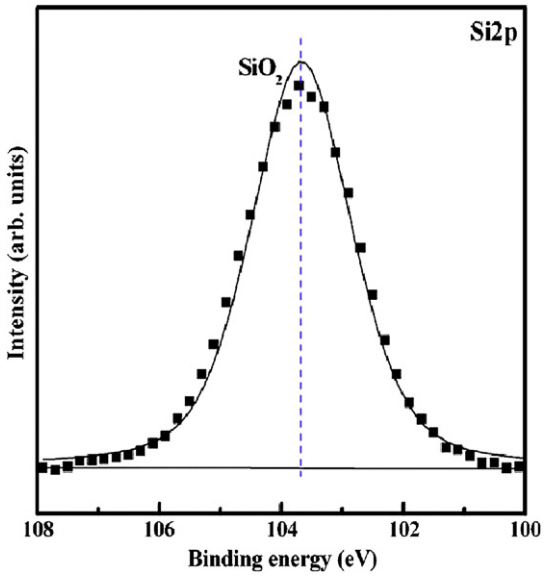

Fig. 8. Deconvoluted high-resolution of Si*2p* obtained on exposed PHPS derived SiO_2 coating, AO fluence = 9.3×10^{20} atoms·cm^{-2}.

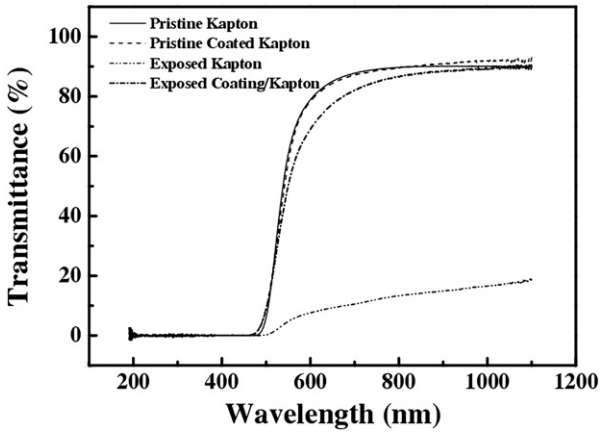

Fig. 9. UV–vis curves of pristine and coated Kapton before and after AO exposure, AO fluence = 9.3×10^{20} atoms·cm^{-2}.

3.3. AO erosion mechanism

In order to better understand the AO erosion resistance of the PHPS derived SiO_2 coating, it is necessary to compare its erosion yield with that of SiO_2 and Al_2O_3 coatings deposited by sol–gel method or plasma sputtering. As it can be seen from Table 2, the erosion yield of the conventional coatings of SiO_2 or Al_2O_3 is in the range of 10^{-25}–10^{-26} cm^3·atom^{-1}, being one or two orders of magnitude lower than that of the polymers substrates (~10^{-24} cm^3·atom^{-1}). Previous experimental results implied that these coatings might crack during AO exposure, undercutting erosion of the polymer substrates could be found in the crack regions of the exposed samples [7,8,11]. In contrast, the PHPS derived SiO_2 coating investigated in this study shows a relatively lower erosion yield of ~10^{-27} cm^3·atom^{-1}. Under the similar conditions of AO exposure, the PHPS derived SiO_2 coating has not exhibited surface cracking or undercutting erosion, Therefore, this PHPS derived SiO_2 coating possesses better AO erosion resistance compared with other kinds of SiO_2 coatings.

Usually, hydroxides appear as intermediate products in the process of sol–gel coating deposition. For example, in the preparation of sol–gel SiO_2 coatings [8], the SiO_2 formation involves in $SiCl_4 \rightarrow Si(OH)_4 \rightarrow SiO_2$. In the conventional sol–gel silica coating, there is silanol ($Si(OH)_4$) remained. During AO exposure, this remained silanol ($Si(OH)_4$) translates to SiO_2 and water vapor. When the generated water vapor evaporates from the coating, volume shrinkage occurs. Thus, these sol–gel coatings usually crack and the polymer substrate suffers undercutting erosion during AO exposure [11,29]. Comparably, the PHPS precursor has a lower chemical stability, even directly translate to SiO_2 in air environment (Eq. (4)), so there is negligible silanol remaining in the PHPS derived SiO_2 coating. As mentioned above, the PHPS derived SiO_2 coating is composed of the SiO_2-rich top layer and the inner PHPS organic layer. The inert SiO_2-rich top layer can play an AO erosion resistant role. If physical defects such as cracks and pin-holes form in this SiO_2-rich top layer during AO exposure or in other operations, the inner PHPS organic layer can prevents propagation of cracks from the SiO_2-rich top layer to the substrate. On the other hand, the inner organic layer containing free Si component can be oxidized to further form a SiO_2-rich surface layer (see Eqs. (4) and (5) [9]. As a result, the physical defects can be healed, which retards the rapid AO erosion of the underlying part of the coating or the substrate. Thus, due to no surface shrinkage induced cracking and the self-healing ability, the PHPS derived SiO_2 coating possesses better AO erosion resistance than conventional sol–gel silica coatings.

$$-[SiH_2\text{–}NH]- + 2O \rightarrow SiO_2 + NH_3 \quad (4)$$

Table 2
Comparisons of AO erosion yield of several protective coatings.

Coating	Preparation method	Precursor	AO fluence (atoms·cm^{-2})	Erosion yield (cm^3·atom^{-1})	Reference
Al_2O_3	Sol–gel	Al $(OC_3H_7)_3$	3.6×10^{20}	2.5×10^{-25}	[7]
SiO_2	Plasma deposition	—	2.0×10^{21}	6.0×10^{-26}	[3]
SiO_2	Sol–gel	$SiCl_4$	2.4×10^{20}	5.9×10^{-26}	[8]
SiO_2	Sol–gel	PHPS	9.3×10^{20}	6.0×10^{-27}	This study

$$Si_{free} + 2O \rightarrow SiO_2 \quad (5)$$

4. Conclusions

In this study, a PHPS derived SiO_2 coating was deposited on Kapton substrate using surface sol–gel method and its AO erosion resistance has been evaluated in a ground-based AO simulator. The experimental results indicate that the PHPS derived SiO_2 coating can protect Kapton effectively from AO attacks. After superficially applied this coating, the erosion yield of Kapton decreases from 3.0×10^{-24} cm^3·atom^{-1} to 6.0×10^{-27} cm^3·atom^{-1}, and the exposed surface morphology changes from “carpet-like” structure to a smooth surface. During AO exposure, the PHPS derived SiO_2 coating shows no surface shrinkage induced cracking due to the direct transformation of PHPS to SiO_2 in the AO beam. On the other hand, this coating possesses self-healing ability, can prevent the undercutting erosion induced by surface defects.

References

[1] M.R. Reddy, J. Mater. Sci. 30 (1995) 281.
[2] P. Gary, Prog. Org. Coat. 47 (2003) 424.
[3] D.G. Zimcik, M.R. Wertheimer, K.B. Balmain, R.C. Tennyson, J. Spacecr. Rockets 28 (1991) 652.
[4] S. Packirisamy, D. Schwam, M.H. Litt, J. Mater. Sci. 30 (1995) 308.
[5] B.A. Banks, A. Snyder, S.K. Miller, K.K. de Groh, J Spacecr. Rockets 41 (2004) 335.
[6] K.K. de Groh, B.A. Banks, J Spacecr. Rockets 31 (1994) 656.
[7] X. Zhang, Y. Wu, G. Liu, S. He, D. Yang, Thin solid Films 516 (2008) 5020.
[8] X. Zhang, Y. Wu, S. He, D. Yang, F. Li, Surf. Coat. Technol. 202 (2008) 3464.
[9] M. Günthner, T. Kraus, A. Dierdorf, D. Decker, W. Krenkel, G. Motz, J. Eur. Ceram. Soc. 29 (2009) 2061.
[10] Y. Iwamoto, K. Sato, T. Kato, T. Inada, Y. Kubo, J. Eur. Ceram. Soc. 25 (2005) 257.
[11] L. Prager, A. Dierdorf, H. Liebe, S. Naumov, S. Stojanović, R. Heller, L. Wennrich, M.R. Buchmeiser, Chem. Eur. J. 13 (2007) 8522.
[12] M. Hasegawa, K. Horie, Prog. Polym. Sci. 26 (2001) 259.
[13] K.W. Lee, S.P. Kowalczyk, J.M. Shaw, Macromol. 23 (1990) 2097.
[14] K.W. Lee, A. Viehbeck, IBM J. Res. Develop. 38 (1994) 457.
[15] S. Duo, M. Li, Y. Zhang, J. Mater. Sci. Technol. 20 (2004) 759.
[16] B.A. Banks, S.K. Rutledge, K.K. de Groh, C.R. Stidham, L. Debauer, C.M. LaMoreaux, NASA, Tech. Memo. 106855 (1995).
[17] S.K. Rutledge, B.A. Banks, F. Difilippo, J. Brady, T. Dever, D. Hotes, LEO NASA Tech. Memo. 100122 (1986).
[18] H. Kriegsmann, G. Engelhardt, Z. Anorg, Allgem. Chem. 310 (1961) 100.
[19] L. Prager, A. Dierdorf, H. Liebe, S. Naumov, S. Stojanović, R. Heller, L. Wennrich, M.R. Buchmeiser, Chem. Eur. J. 13 (2007) 8522.
[20] M. Monti, B. Dal Bianco, R. Bertoncello, S. Voltolina, J. Cult. Herit. 9 (2008) e143.
[21] Y. Iwamoto, K. Kikuta, S. Hirano, J. Mater. Res. 13 (1998) 353.
[22] Y. Iwamoto, K. Kikuta, S. Hirano, J. Mater. Res. 14 (1999) 1886.
[23] D.G. Zimcik, C.R. Maag, J. Spacecr. 25 (1988) 162.
[24] E. Grossman, Y. Lifshitz, J.T. Wolan, C.K. Mount, G.B. Hoflund, J. Spacecr. Rockets 36 (1999) 75.
[25] M.A. Golub, T. Wydeven, R.D. Cormia, Polym. Commun. 29 (1988) 285.
[26] L. Hu, M. Li, C. Xu, Y. Luo, Y. Zhou, Surf. Coat. Technol. 203 (2009) 3338.
[27] Y. Kurokawa, T. Soga, S. Nakata, T.I. Koma, S. Tero-Kubota, J. Mater. Sci. Lett. 17 (1998) 275.
[28] L. Pach, J. Majling, J. Sol–gel, Part. Sci. Technol. 18 (2000) 99.
[29] F. Bauer, U. Decker, A. Dierdorf, H. Ernst, R. Heller, H. Liebe, R. Mehnert, Prog. Org. Coat. 53 (2005) 183.